An Efficient Bidirectional Battery Charger Controller for Electric Vehicles

Nikhitha Madala[1], A Srihari Babu[2] and G Srinivasa Rao[3]

[1]PG Scholar, Department of EEE, VFSTR Deemed to be University, Guntur, India.
[1]Assistant Professor, Department of EEE, VFSTR Deemed to be University, Guntur, India.
[3]Professor, Department of EEE, VFSTR Deemed to be University, Guntur, India.

Abstract: This concept presents EV battery charge management in a power distribution system. For EV safety, new power electronic converter topologies with Inductive Power Transfer (IPT) are employed. For zero current switching, this IPT architecture uses classical series L-C compensation with minimal auxiliary components (ZCS). The suggested architecture provides a consistent output voltage even when the input voltage varies widely. However, the number of active and passive circuit components increases with design complexity. A controlled Bidirectional Battery Charger for EV with Vehicle-to-Grid Capability is suggested to solve this issue. Other key aspects of the suggested charge controller include its active and reactive control in G2V and V2G operation with THD according to international standards, care for battery life time, and smooth power fluctuation in charge and discharge modes. These two EV battery charge controller topologies are confirmed in simulation. Compared to IPT topology, bidirectional converter offers greater advantages.

KEYWORDS:

DOI of the Article: https://doi.org/10.46501/IJMTST0708024

Available online at: http://www.ijmtst.com/vol7issue08.html

As per UGC guidelines an electronic bar code is provided to seure your paper

To Cite this Article: Nikhitha Madala, A Srihari Babu and G Srinivasa Rao. An Efficient Bidirectional Battery Charger Controller for Electric Vehicles. *International Journal for Modern Trends in Science and Technology* 2021, *7*, 0708049, pp. 133-141. https://doi.org/10.46501/IJMTST0708024

Article Info. Received: 09 July 2021; Accepted: 07 August 2021; Published: 14 August 2021

INTRODUCTION

Traditional Internal Combustion (IC) engines run on petroleum fuels (petrol, diesel, or LPG). The most urgent answer is to reduce the usage of fossil fuels as much as possible. Moreover, traditional IC engines produce CO2 and other greenhouse gases, making environmental standards difficult to meet. The solution is to use alternative fuel cars like electric and hybrid electric automobiles (HEV). EV does not produce tailpipe pollutants such particles, ozone, volatile organic compounds, carbon monoxide, hydrocarbons, lead, and oxides of nitrogen. On can also reduce the use of fossil fuels Moreover, the EV market allows humans to extend transportation life expectancy at a cheaper cost. In the past, EVs' market success was limited by battery and power shaping technologies. However, in recent decades, BT has evolved to be more energy dense, lighter, and more efficient.

Short driving ranges require efficient, quick chargers for human safety. In the current environment, inductive power transfer (IPT)-based battery charging (BC) systems are used for EV stationary and dynamic charging. Compensation networks are proposed to reduce circuit impedance and increase converter efficiency. However, the number of active and passive circuit components increases with design complexity. The proper solution extends driving range, reduces maintenance, reduces carbon footprint, and saves money. Thus, converter selection is critical to EV market flow. As a result, it expertly assists reducing environmental difficulties caused by transportation.

CC/CV mode charging in [7] requires a complete bridge DC-DC converter with four switch AC-DC converter. These references make the PFC controller's control circuit more complicated. [8] shows a level 2 charger with a bridgeless boost PFC converter and an isolated phase shifted full bridge DC-DC converter. SiC power switches are used to achieve great density and efficiency. At 200 kHz, maximum efficiency is 95% and THD is 4.2%.

[10] develops an electric scooter on-board battery charger. The charger is designed for a 180 V 12 Ah lead-acid battery and works with a 110 V 60 Hz single phase outlet. The LDC idea is suggested. A DC-DC converter is suggested to charge a 12V auxiliary battery from a 180V propulsion battery.

[13] proposes a Buck PFC converter with constant on-time control.

The suggested design is tested for 100 W using a 90 V supply. The design complies with IEC61000-3-2. With full load and universal voltage, the efficiency is 0.96. Because of the discontinuous input current, a big filter is required at the input.

[14] proposes a two-switch Boost-interleaved buck-boost architecture.

The proposed converter has less voltage stress on the switches and less conduction loss in the switch and inductor. A 93 percent efficiency is achieved with a low THD universal line voltage input. In this view, IPT with auxiliary circuit can minimise problems in VSI-fed converter network.

This article proposes a topology that uses classical series L–C compensation with tiny auxiliary components to create ZVS (ZCS). The suggested architecture provides a consistent output voltage even when the input voltage varies widely. The output current can be readily regulated by the input voltage, eliminating the need for a high-power processor and lowering the converter's cost.

The suggested architecture provides a consistent output voltage even when the input voltage varies widely. However, the number of active and passive circuit components increases with design complexity. A controlled Bidirectional Battery Charger for EV with Vehicle-to-Grid Capability is suggested to solve this issue. Its key features are as follows: (2) concern for battery life time, showing smooth power variation in charge and discharge modes; (3) control strategy of the charge equalisation circuit is completely incorporated into the charger control algorithm

IPT BASED BATTERY CHARGER TOPOLOGY

Fig. 1 depicts the suggested architecture in which two stages of the converter are controlled independently by MPWM. To accomplish zero-voltage zero-current switching (ZVZCS), the pulses are generated at 5 kHz switching frequency in MPWM mode.

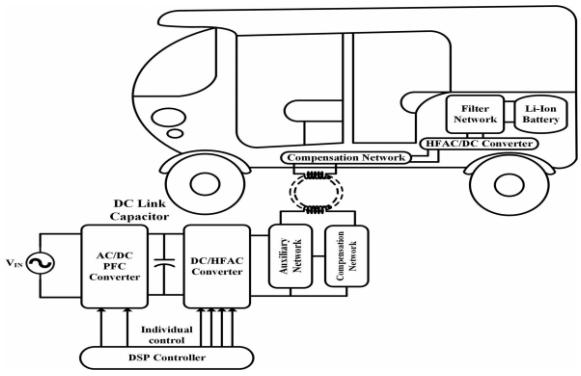

Operating Principle:

A H-bridge is formed of active switches S1–S4 and diodes D5–D8 (conventional). Ca1 and Ca2 also function as potential dividers at the input with supplementary LA and TA to keep the circuit soft-switching with BC. The circuit's primary and secondary sides are connected through L1 and L2. [22] uses MPWM to regulate the converter's functioning.

The following assumptions are made to comprehend the proposed converter's operation.

1) All active and passive devices including transformer, dc source, switches, diodes, and capacitors are suitable.

2) Inductor series resistance and transformer inter winding capacitance are ignored.

3)Capacitors (Ca, Ca1, Ca2) and CF are big enough to maintain constant voltage at the converter's input and output.

4) The magnetising inductance of TA is ignored.

Operation of Proposed Converter

The operating principle of the proposed topology in steady state is divided into eight modes (modes I–VIII) as shown in Fig. 4.2 and the operating waveforms are shown in Fig. 4.3.

1) Mode I (t0 ≤t<t1), Fig. 2(a): Before time instant *t*0, lagging current (*IL*1 + *ILA*) is flowing from *D*1 and *S*2, Therefore, at *t*0 instant, the switch *S*1 is turned ON with ZVS. Furthermore, a potential difference between *AC* and *CB* is created and current *ILA* start rising from *ILA*(*t*0)

$$i_{L_A} = \begin{cases} \dfrac{|V_{Ca1} - V_{Ca2}|}{2L_A} T_{ON} - i_{L_A}(t_0) & \text{If} \rightarrow R_{ON(S_1-S_4)} \neq 0 \\ |V_{Ca1} - V_{Ca2}| = 0 \;||\; i_{L_A} = 0 & \text{If} \rightarrow R_{ON(S_1-S_4)} = 0 \end{cases} \quad (1)$$

2) Mode II (t1 ≤ t < t2), Fig. 2(b) and (c): Before *t*0, switch *S*1 is conducting and switch current difference (*iS*1− *iS*2) is flowing from *TA* (*ITA*1 + *ITA*2 = *ILA*).

Applying KCL at points *A* and *B* and using low energy Conservation

$$i_{C_{S1}} + i_{C_{S4}} = i_{T_{A2}} + i_{L_1} \quad (2)$$

$$2i_{C_{S1}} = i_{L_1} + \frac{i_{L_A}}{2}. \quad (3)$$

At the starting of this mode, *S*1 is turned OFF when *S*3, *S*4 are already OFF, and *S*2 is still conducting. The dominant inductance *L*1 is now in cutoff from dc power source, and *IL*1 + *ILA*2 starts charging switch peracetic capacitor *CS*1. At instant *t*11, *VCS*1 reaches *VDC*. After *t*11, *IL*1 finds a path by forcing the change in *ILA*. The inductor *LA* rejects this change and a current starts from *S*2 to *S*4, which discharges *CS*4. After *CS*4 voltage reaches zero,*D*4 turns ON and this freewheeling results in the decrement of *IS*2 to zero or ZCS for switch *S*2

$$t_{(V_{CS1}=V_{DC})} = \frac{\frac{1}{2}C_{S3}V_{DC} - \left(i_{L_1(t_{1-})} + \frac{i_{L_A(t_{1-})}}{2}\right)}{i_{L_1(t)} + \frac{i_{L_A(t)}}{2}}. \quad (4)$$

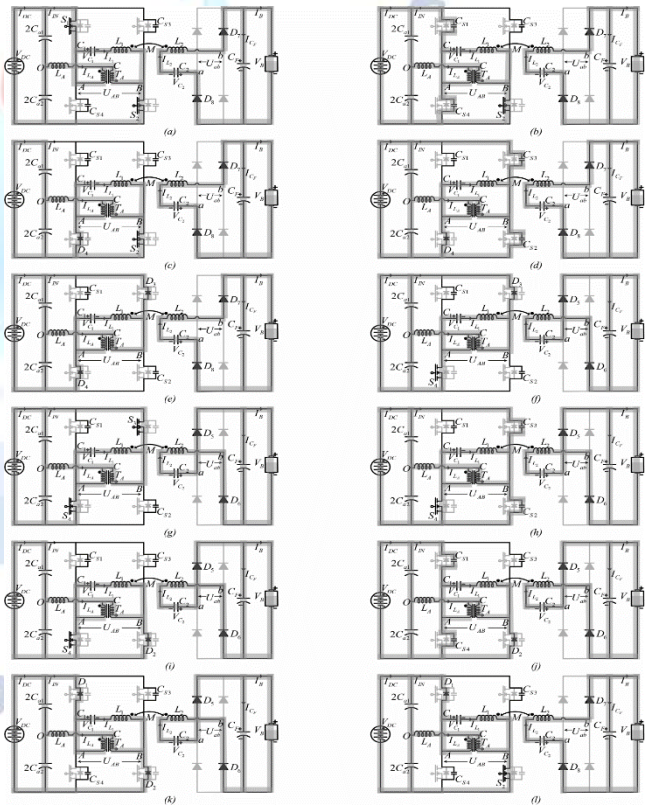

Fig. 2. Operating modes of proposed battery charger topology

3) Mode III (t2 ≤ t < t3), Fig. 2(d) and (e): This mode starts from *S*2 ZCS turn OFF while other switches are already OFF. During this mode, the peracetic capacitor *CS*2 starts charging till *t*21 up to *VDC* and the current *ILA* decrementing toward zero after attaining its positive

peak. After *t*21, the current *IL*1 +*ILA*2 finds its path by discharging capacitors *CS*3, *CS*4 and turns ON the diodes *D*2, *D*4

$$t_1 > 2C_{S1}\frac{V_{DC}}{i_{L_1(t_0)} + \frac{i_{L_A(t_0)}}{2}}. \qquad (5)$$

The voltage stress across switch is given by the following expression:

$$v_{S1} = V_{DC} + v_{C_1} \qquad (6)$$

$$v_{S4} = -v_{C_1}. \qquad (7)$$

*4) Mode IV (t*3 ≤*t*<*t*4*), Fig. 2(f):* In this mode of operation, *S*4 is turned ON with ZVS as *D*4 is on and the voltage across *S*4 is near zero. The auxiliary inductor current *ILA* is increasing linearly in a positive direction after attaining its negative peak.

*5) Mode V (t*4 ≤ *t* < *t*5*), Fig. 2(g):* In this mode, *S*3 is turned ON with ZVS. *IAB* starts following the sinusoidal wave shape, and voltage across *S*3, *S*4 are zero as its path got completed.

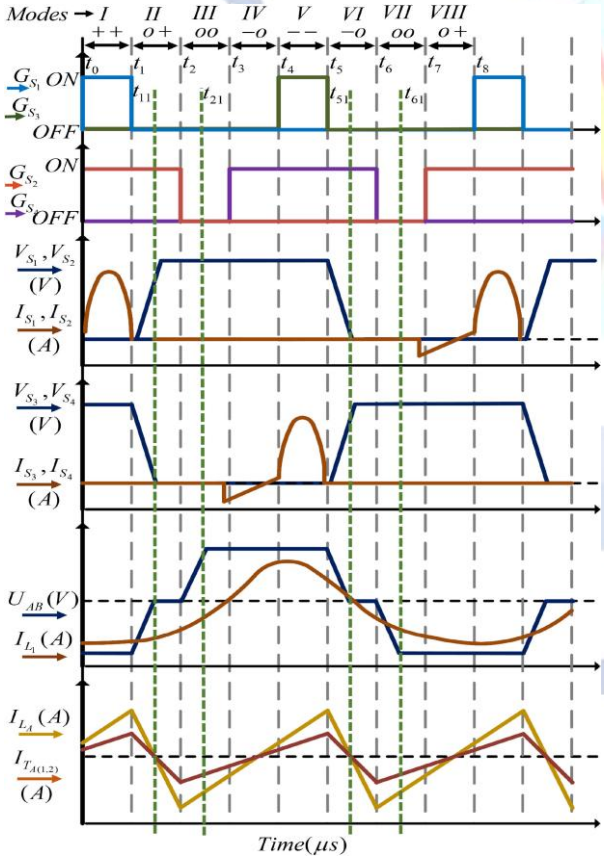

Fig. 3. Theoretical operating waveform of proposed wireless converter topology.

*6) Mode VI (t*5 ≤ *t* < *t*6*), Fig. 2(h) and (i):* This mode starts by turning OFF *S*3,which triggers *CS*3 charging up to *VDC* at *t*51. The auxiliary inductor current *ILA* is decreasing after attaining its peak and *IL*1 , *ILA* forces *IS*4 to reduce for ZCS turn-OFF condition.

*7) Mode VII (t*6 ≤ *t* < *t*7*), Fig. 2(j) and (k):* In this mode, *S*4 turned OFF at ZCS and *VCS*4 rises up to *VDC* at *t*61. After *t*61, *ILA* starts incriminating in positive direction. The diodes *D*1 and *D*2 turned ON and power is feedback to the source.

*8) Mode VIII (t*7 ≤ *t* < *t*8*), Fig. 2(l):* During this mode of operation, switch *S*2 is turned ON with ZVS and current shifts from *D*2 to *S*2. During mode, I to VIII constant voltage and current are maintained in the battery.

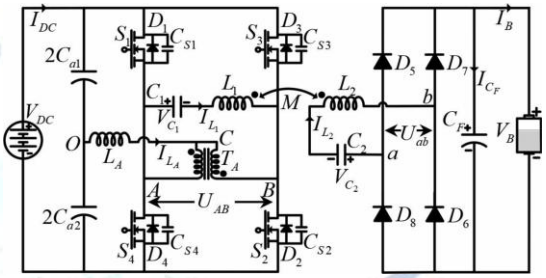

Fig. 4. Proposed network configuration of EV battery charger

BATTERY CHARGER TOPOLOGY WITH G2V AND V2G OPERATION

PEVs and their chargers are projected to become more important grid components. Chargers and their accompanying sophisticated management systems are critical components in making PEVs competitive with ICE cars. Not controlled rectifiers, inverters, filters and DC/DC converters are common. The regulation of active power, reactive power, and voltage in these power converters has also been studied. In terms of topological designs, our idea resembles those in as well as the controller's approach. In addition to [11], [12], and [20], this work proposes a reduced-scale experimental setup to show appropriate and stable functioning. Also, the mechanical assembly of all components to create the final product showed to be crucial [16].

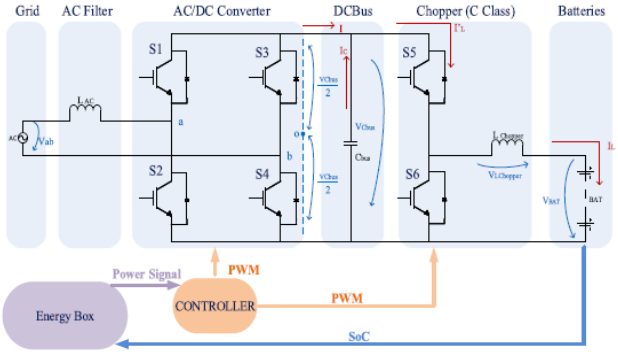

Fig. 5. PEV charger topology

The topology presented in Fig. 5 is formed by three legs of two Insulated Gate Bipolar Transistors (IGBT), denoted by $Sj \in \{1, \ldots, 6\}$. The IGBTs are used due to their good compromise characteristics associated with voltage, switching frequency and current limits.

DC/DC Converter Circuit Analysis

The DC/DC converter is a C class chopper (i.e., positive voltage and positive and negative current). The key operation equations for buck and boost modes are (1) to (4) and (5) to (8).

$$V_{BAT} = V_{Cbus} - L_{Chopper} \cdot \frac{dI_L}{dt} \quad (1)$$

$$I_L = \frac{1}{L_{Chopper}} \cdot \int_0^{Ton} (V_{Cbus} - V_{BAT})\, dt \quad (2)$$

$$V_{BAT} = -L_{Chopper} \cdot \frac{dI_L}{dt} \quad (3)$$

$$I_L = \int_{Ton}^{Toff} -\frac{V_{BAT}}{L_{Chopper}} dt \quad (4)$$

$$V_{BAT} = L_{Chopper} \cdot \frac{dI_L}{dt} \quad (5)$$

$$I_L = \frac{1}{L_{Chopper}} \cdot \int_0^{Ton} V_{BAT}\, dt \quad (6)$$

$$V_{BAT} + V_{LChopper} = V_{Cbus} \quad (7)$$

$$I_L = \frac{1}{L_{Chopper}} \cdot \int_{Ton}^{Toff} (V_{BAT} - V_{Cbus})\, dt \quad (8)$$

Each power switch has its own switching period (T), which is formed by the driving (Ton) and cut-off (Toff) periods. To get the voltage conversion ratio, divide the duty-cycle (D) by the voltage conversion ratio (V) [26].

$$D = \frac{T_{on}}{T} \quad (9)$$

$$V_{BAT} = V_{Cbus} \cdot \frac{T_{on}}{T} = V_{Cbus} \cdot D \quad (10)$$

$$\frac{1}{1-D} = \frac{V_{Cbus}}{V_{BAT}} \Leftrightarrow D = -\frac{V_{BAT}}{V_{Cbus}} + 1 \quad (11)$$

$$V_{BAT} = V_{Cbus} \cdot (1 - D) \quad (12)$$

This converter's functioning is determined by the inductor (LChopper) and the DC bus capacitor (Cbus). The inductor controls the source current ripple and mitigates some higher switching frequency effects [26]. It should be designed for increased power output when the battery voltage is lower, regardless of operation mode. Equation (13) yields the buck mode:

$$L_{Chopper} = \frac{V_{Cbus} - V_{BAT_{nom}}}{2 \cdot \Delta I_L} \cdot T_{on} \quad (13)$$

AC/DC Converter Circuit Analysis

To accomplish the desired charger characteristics, an AC/DC converter (Fig. 1) was utilised as a regulated rectifier and an inverter for G2V and V2G operating modes. Power switch drive control allows AC or DC voltage flexibility, lower voltage ripple and greater efficiency for each operating mode (given the lower internal IGBT resistance and the unipolarPWM generation method). To meet the Kirchoff voltage rule, the switches on the same leg (see Fig. 1) are not switched on at the same time, giving the condition S1 + S2 = 1. A voltage fluctuation between VCbus 2 and –Vcbus 2 is enabled (see Fig. 1). Vbn is the output voltage from phase a to point n. Vno is the neutral voltage between n and the DC bus's midpoint. By comparing the switching pulses of devices to modulation signals, the Fourier series approximates the switching function of devices to 12 (1 + mi) (triangularwaveform). The carrier signal is compared to the modulation signal (sinusoid) and its symmetric to turn each IGBT on and off. Table I shows the outcomes of this comparison. (19) gives the output voltage's basic component:

$$\begin{cases} V_{ab} = m_i \cdot V_{Cbus} \text{ if } m_i \le 1 \\ V_{Cbus} < V_{ab} < \frac{\pi}{4} \cdot V_{Cbus} \text{ if } m_i > 1 \end{cases} \quad (19)$$

TABLE I
UNIPOLAR INVERTER RULES

S_1	S_2	S_3	S_4	V_{an}	V_{bn}	$V_{ab} = V_{an} - V_{bn}$
on	–	–	on	V_{Cbus}	0	V_{Cbus}
–	on	on	–	0	V_{Cbus}	$-V_{Cbus}$
on	–	on	–	V_{Cbus}	V_{C_bus}	0
–	on	–	on	0	0	0

To simplify circuit analysis, the chopper controller design assumes high capacities on both sides of the chopper, low L capacity (relative to Cbus capacity), and minimal switching losses. To develop the control rules, Kirchhoff differential equations characterising the converter's energy requirement (see (21)–(24)) were determined. As shown in Fig. 6, two voltage PI chopper controllers are produced.

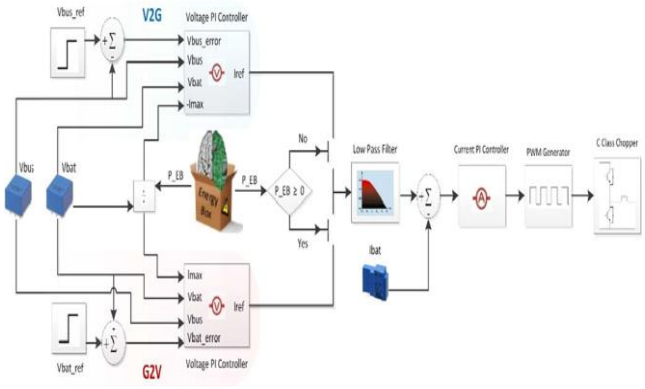

Fig. 6. DC/DC converter controller architecture for V2G and G2V operation modes, respectively

The AC/DC converter controller used as an inverter uses only unipolar switching. A PLL provides a unit sinusoid reference synced with the voltage grid. The chopper limited the available DCbus power in this mode, thus only properly inverting the DCbus voltage was required. Fig. 7 shows both AC/DC converter controllers.

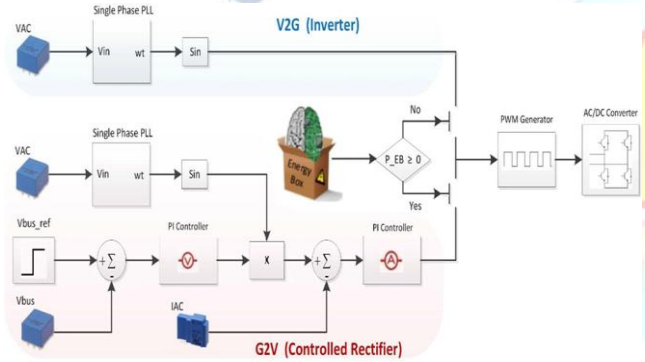

Fig. 7. AC/DC converter controller architecture for V2G and G2V operation modes.

SIMULATION RESULTS

Simulation Results of the Inductive Power Transfer Topology for Electric Vehicle Battery Charging:

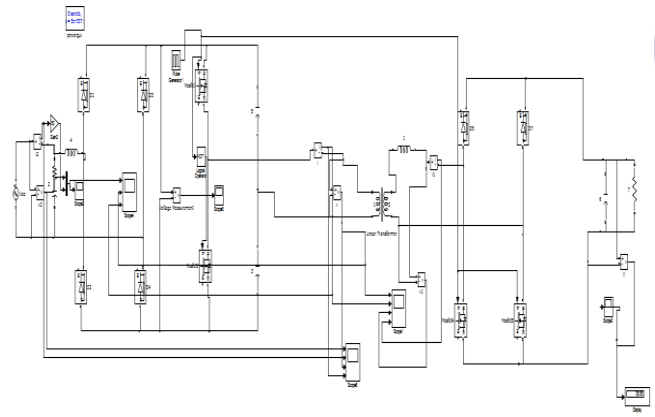

Fig 7 Simulink diagram of Inductive Power Transfer Topology for Electric Vehicle Battery Charging

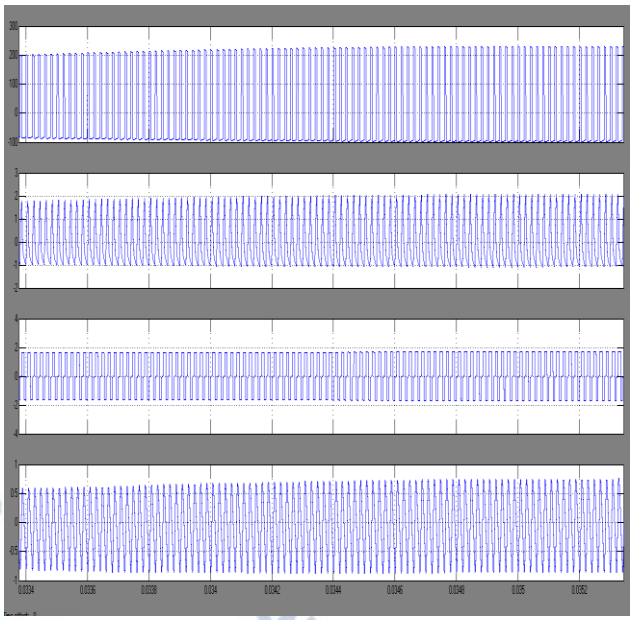

Fig. 8.Simulation waveforms over a complete line cycle, input ac voltage (VAC) and current (IAC) and transformer primary voltage (VP) and current (IP)

Fig. 8 shows the measured waveforms of the line input voltage and current, and the transformer main voltage and current. Fig. 9 (DCM) and Fig. 10 (CCM) show the transformer primary and secondary voltage and current waveforms zoomed in to validate the intended functioning. In Fig. 10, the primary voltage waveform shows a reduction in voltage due to the finite values of bus capacitors C1 and C2.

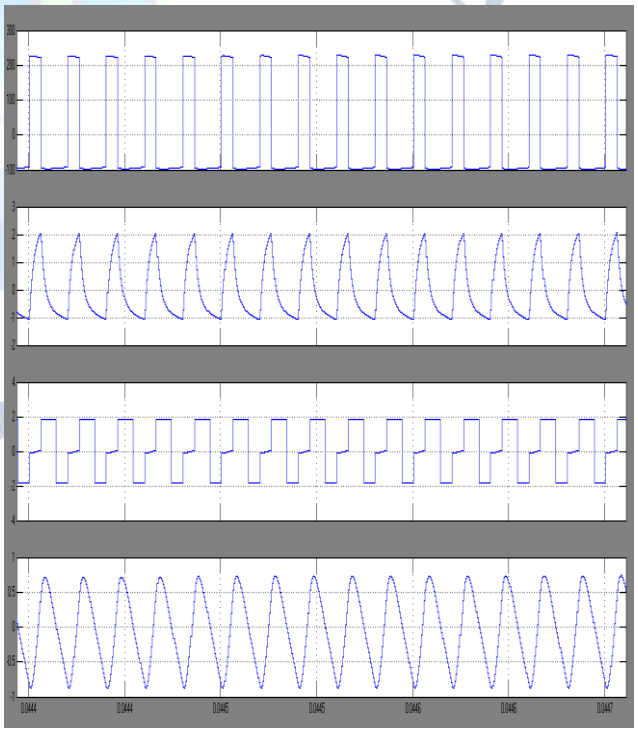

Fig. 9. Measured waveforms from zero crossingand operating in DCM mode. Transformer primary voltage (VP) and current(IP) and secondary voltage (VS) and current (IS).

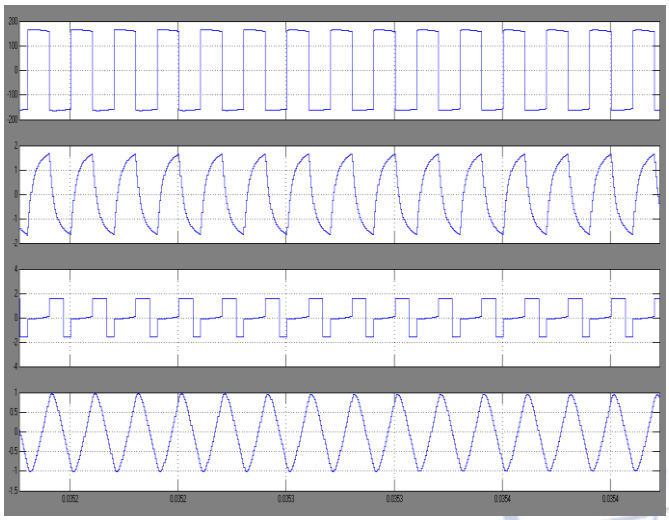

Fig. 10.Simulation waveforms operating in CCM mode.Transformer primary voltage (VP) and current(IP) and secondary voltage (VS) and current (IS).

Simulation Results of Proposed Battery Charger Topology with G2V and V2G Operation

The described Non–Isolated Bi-directional DC-DC converter is simulated using MATLAB/Simulink for both G2V and V2G operation.. The detailed results are shown below.

G2V Mode

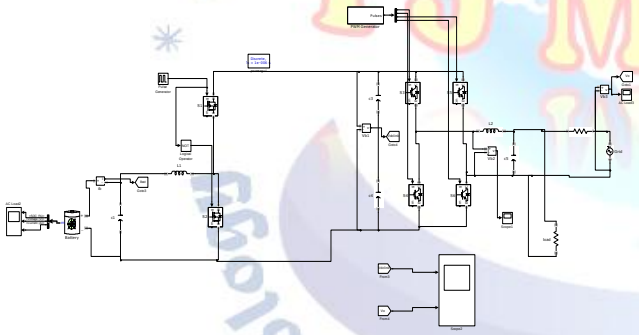

Fig 11 Simulation diagram of G2V mode

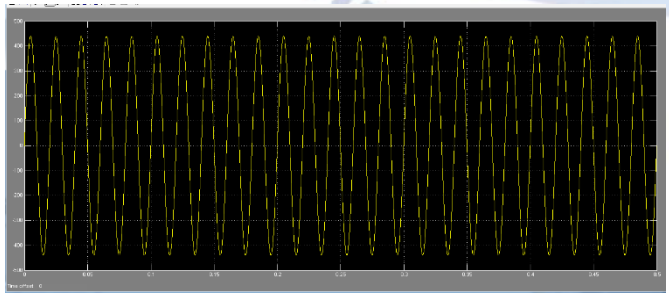

Fig 12 Simulation results of grid voltage

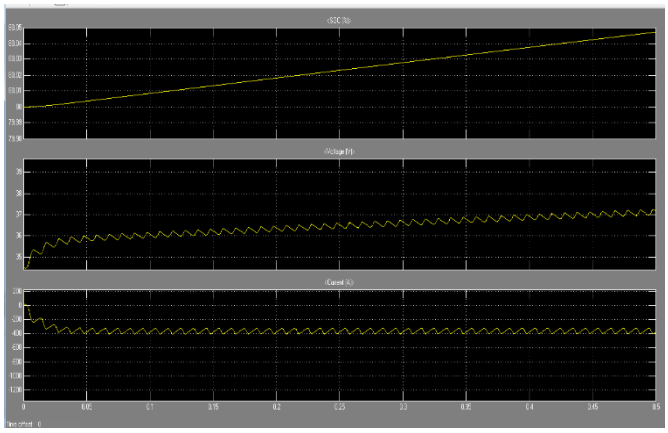

Fig 13 Simulation results of battery (a) Battery SOC, (b) Battery voltage, (c) Battery current

Fig 11 is a G2V simulation circuit. Figures 12 and 13 illustrate the simulation results for G2V mode. The results are highlighted on the four main points. The simulation replaces the battery with its equivalent resistance, which is the voltage to current ratio. The battery is charged from 35 V to 37 V in 0 to 0.5 sec. The battery is charging and shows a –ve current, indicating it is charging. The voltage ripple is restricted to 0.3 V peak-to-peak.

V2G Mode

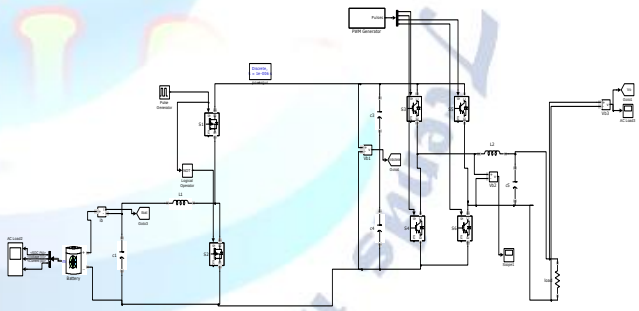

Fig 14 Simulation diagram of V2G mode

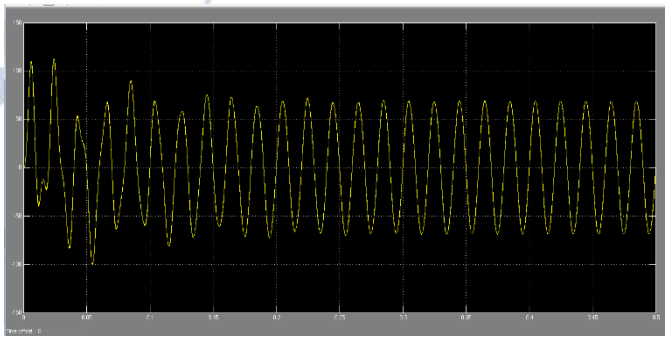

Fig 15 Simulation results of load volatge

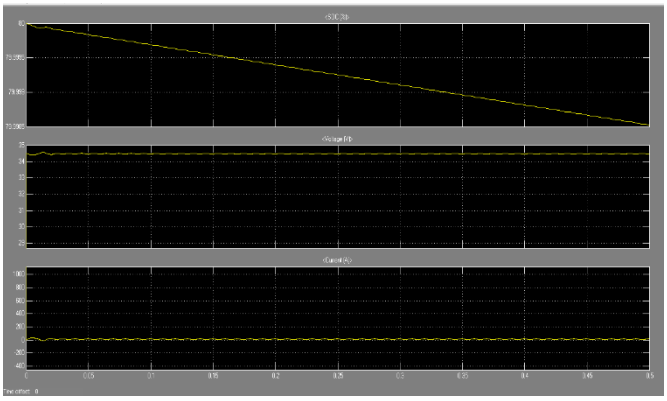

Fig 16 Simulation results of battery (a) Battery SOC, (b) Battery voltage, (c) Battery current

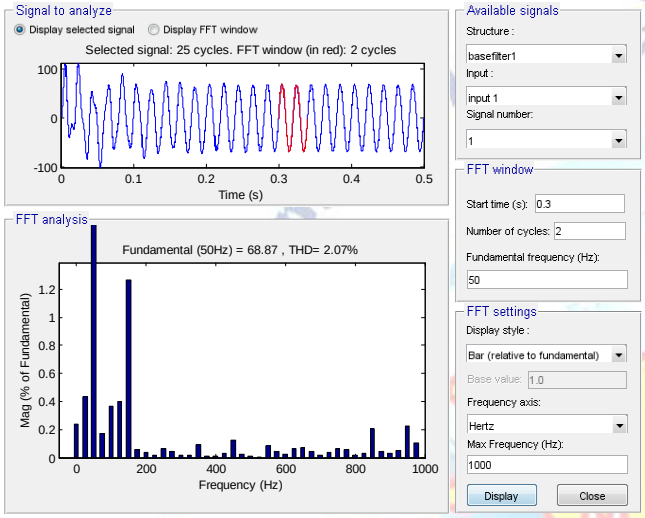

Fig 17 THD analysis of V2G

In V2G mode, the DC-DC converter works as a Boost converter, supplying power to the DC connection for additional use. The simulation uses 230 V nominal battery voltage and 420 W reference power. With the controller's current reference and two switches regulated, the desired power flow is maintained.

CONCLUSION

A 230 V charger for electric vehicles is designed for level 1 charging. The phases and problems of an electric vehicle charger are explained. The changes were made to address significant problems. A two-stage charger featuring an active PFC converter and a bidirectional DC-DC converter is designed. At maximum load, the active PFC produces less than 5% THD. The PFC converter also works with a wide range of loads. The simulated findings are used to analyse the power stage and controller architecture. The charging current and voltage are regulated by a second stage DC-DC converter. The converter charges the propulsion battery in CC/CV mode across a large voltage range. A V2G controller for the DC-DC converter was designed to feed electricity from the propulsion battery to the grid. Using the same Electric Vehicle charger, a new Low-Voltage DC-DC converter is suggested to charge the Auxiliary battery. The battery voltage and current waveforms are shown, and the converter's performance is checked.

REFERENCES

[1] S. B. Peterson, J. Whitacre, and J. Apt, "The economics of using plug-in hybrid electric vehicle battery packs for grid storage," J. Power Sources, vol. 195, no. 8, pp. 2377–2384, 2010.

[2] Y. Zhou, M. Wang, H. Hao, L. Johnson, and H. Wang, "Plug-in electric vehicle market penetration and incentives: A global review," Mitigation Adaptation Strategies Global Change, vol. 20, no. 5, pp. 777–795, 2015.

[3] B. Nykvist and M. Nilsson, "Rapidly falling costs of battery packs for electric vehicles," Nature Climate Change, vol. 5, no. 4, pp. 329–332, 2015.

[4] W. Zhang and C. C. Mi, "Compensation topologies of high-power wireless power transfer systems," IEEE Trans. Veh. Technol., vol. 65, no. 6, pp. 4768–4778, Jun. 2016.

[5] Y. Jiang, L.Wang, Y.Wang, J. Liu, X. Li, and G. Ning, "Analysis, design, and implementation of accurate ZVS angle control for EV battery charging in wireless high-power transfer," IEEE Trans. Ind. Electron., vol. 66, no. 5, pp. 4075–4085, May 2019.

[6] O. C. Onar,M. Chinthavali, S. L. Campbell, L. E. Seiber, and C. P. White, "Vehicular integration of wireless power transfer systems and hardware interoperability case studies," IEEE Trans. Ind. Appl., vol. 55, no. 5, pp. 5223–5234, Sep./Oct. 2019.

[7] G. N. B. Yadav and N. L. Narasamma, "An active soft switched phaseshifted full-bridge dc–dc converter:Analysis, modeling, design, and implementation," IEEE Trans. Power Electron., vol. 29, no. 9, pp. 4538–4550, Sep. 2014.

[8] V. R. K. Kanamarlapudi,B.Wang, P. L. So, and Z.Wang, "Analysis, design, and implementation of an APWM ZVZCS full-bridge dc–dc converter for battery charging in electric vehicles," IEEE Trans.Power Electron., vol. 32, no. 8, pp. 6145–6160, Aug. 2017.

[9] J. K. Nama, M. Srivastava, and A. K. Verma, "Modified inductive power transfer topology for electrical vehicle battery charging using auxiliary network to achieve zero-voltage switching for full load variations," IET Power Electron., vol. 12, no. 10, pp. 2513–2522, 2019.

[10] A. Soares, H. Melo, C. H. Antunes, J. P. Trovao, A. Gomes, and H. Jorge, "Integration of the electric vehicle as a

manageable load in a residential energy management system," in *Proc. IEEE Veh. Power Propulsion Conf.*, Montreal, QC, Canada, 2015, pp. 1–6.

[11] H. N. Melo, J. P. Trov˜ao, P. G. Pereirinha, and H. Jorge, "Electric vehicles' intelligent charger for automated energy management system," in *Proc. Int. Workshop Energy Efficiency More Sustain. World*, Azores, Portugal, 2012, pp. 1–6.

[12] H. N. Melo, J. P. Trov˜ao, C. H. Antunes, P. G. Pereirinha, and H. Jorge, "An outlook of electric vehicle daily use in the framework of an energy management system," *Manag. Environ. Qual.: Int. J.*, vol. 26, no. 4, pp. 588–606, 2015.

[13] H. N. Melo, J. P. Trov˜ao, P. G. Pereirinha, and H. Jorge, "Energy profits with controllable electric vehicle's charger under energy box decisions," in *Proc. 7th Int. Conf. Energy Efficiency Domestic Appliances Lighting*, Coimbra, Portugal, 2013, pp. 1–6.

[14] V. Monteiro, J. P. Carmo, J. G. Pinto, and J. L. Afonso, "A flexible infrastructure for dynamic power control of electric vehicle battery chargers," *IEEE Trans. Veh. Technol.*, vol. 65, no. 6, pp. 4535–4547, Jun. 2016.

[15] I. Vittorias, M. Metzger, D. Kunz, M. Gerlich, and G. Bachmaier, "A bidirectional battery charger for electric vehicles with V2G and V2H capability and active and reactive power control," in *Proc. IEEE Transp. Electrific. Conf. Expo*, Dearborn, MI, USA, 2014, pp. 1–6.

[16] M. I. Milan´es-Montero, M. A. G. Mart´ınez, E. Gonz´alez-Romera, E. Romero-Cadaval, and F. Barrero-Gonz´alez, "Active and reactive power control strategies for electric vehicles in smart grids," in *Proc. 10th Int. Conf. Compat., Power Electron. Power Eng.*, Bydgoszcz, Poland, 2016, pp. 114–119.